Rare Met. (2015) 34(5):301–307
DOI 10.1007/s12598-014-0297-0

RARE METALS
www.editorialmanager.com/rmet

# Sonochemical synthesis and characterization of uniform lanthanide orthophosphate ($LnPO_4$, Ln = La and Ce) nanorods

**Anukorn Phuruangrat*, Titipun Thongtem, Somchai Thongtem***

Received: 18 December 2013 / Revised: 15 February 2014 / Accepted: 21 April 2014 / Published online: 4 June 2014


**Abstract** Uniform lanthanide orthophosphate ($LnPO_4$, Ln = La and Ce) nanorods were successfully synthesized by a simple ultrasonic irradiation method using lanthanide nitrate salt ($Ln(NO_3)_3{\cdot}6H_2O$, Ln = La and Ce) and sodium phosphate ($Na_3PO_4$) in aqueous solutions with the pH of 1–3. The products were characterized by X-ray diffraction (XRD), scanning electron microscopy (SEM), transmission electron microscopy (TEM), high-resolution transmission electron microscopy (HRTEM), Fourier transform infrared spectrometer (FT-IR), and UV–visible (UV-Vis) spectroscopy. In this research, the products are nanorods of monoclinic $LaPO_4$ and hexagonal $CePO_4$ structures and the vibration modes of $PO_4^{3-}$, including the strong peaks at 227 nm for $LaPO_4$, and at 225 and 278 nm for $CePO_4$.

**Keywords** Lanthanide orthophosphate; Nanorods; Ultrasonic irradiation

## 1 Introduction

According to the $LnPO_4$, Ln = La,…, and Gd of the periodic table of the elements, lanthanide phosphate compounds, the important family members of the rare-earth compounds, have increasing attention and application as luminescent materials, moisture sensors, heat-resistant materials, hosts for radioactive nuclear wastes, photocatalytic materials, and energy fuels. They have their particular 4f–5d and 4f–4f electronic transitions which are different from other elements [1–5]. Among them, $LnPO_4$ (Ln = La and Ce) are materials of this group which can be applied for luminescent lamps as highly efficient emitters of green light. Even below the temperature of 1,200 K, monoclinic $CePO_4$ remains as a stable compound which makes it as useful high-temperature material and as a number of applications. There are two polymorphs, which are designated as monoclinic and hexagonal $CePO_4$ structures. The monoclinic $CePO_4$ can be applied as heat-resistant and ceramic materials, while the hexagonal $CePO_4$ can be functioned for tribology applications [2, 6–8]. $LaPO_4$ and its solid solutions are able to be employed in luminescent lamps as highly-efficient emitters of green light. Monoclinic monazite $LaPO_4$ is one of the most stable materials even at high temperature. It is applied in ceramic composites (CMCS) and in optoelectronic domains [7, 9].

There are many synthetic methods to produce 1D $LaPO_4$ and $CePO_4$ nanostructures such as microemulsion [2, 10], solid-state reaction [4], hydrothermal [3, 8, 9], and slow-cooling [11]. These methods require the use of high temperatures, special conditions, tedious procedures, catalytic materials, and templates. Thus, the development of practical methods for producing a large numbers of 1D nanostructure at low cost is still a great challenge for future study. Chemical methods seem to provide an alternative and intriguing strategy for producing 1D nanomaterials with respect to material diversity, cost, versatility, synthetic tenability, and potential for large scale production. In the past few decades, nanomaterials with controlled shapes and sizes were synthesized and

A. Phuruangrat*
Department of Materials Science and Technology, Faculty of Science, Prince of Songkla University, Hat Yai, Songkhla 90112, Thailand
e-mail: phuruangrat@hotmail.com

T. Thongtem
Department of Chemistry, Faculty of Science, Chiang Mai University, Chiang Mai 50200, Thailand

S. Thongtem*
Department of Physics and Materials Science, Faculty of Science, Chiang Mai University, Chiang Mai 50200, Thailand
e-mail: schthongtme@yahoo.com

applied in many areas such as catalysis, optics, electronics, ceramics, and magnetics. Different shapes usually display different surfaces which cause different active planes to be exposure. Their sizes, surfaces, and particle interactions have the influence on some unique properties and performances of nanomaterials. Thus, it is important to look for the controllable synthesis of nanomaterials [12]. However, a sonochemical method was regarded as an effective route for the production of high quality anisotropic nanomaterials. The sonochemical process was proved to be an available technique to obtain novel materials and to produce nanomaterials with unique morphology and unusual properties. During sonication, propagation of pressure wave is intense enough to make the formation, growth, and implosive collapse of bubbles in a liquid medium. During acoustic cavitation, these bubbles generate localized hot spots, which have an extremely high temperature (>5,000 K), pressure (>20 MPa), and cooling rate ($1 \times 10^{10}$ K·s$^{-1}$). Thus, the sonication process provides an ideal route for the preparation of nanomaterials. The advantages of this method include a rapid reaction rate, controllable reaction condition, and the ability to form materials with uniform shape, narrow size distribution, and high purity [13–15]. There are many reports on the synthesis of nanomaterials by sonochemical method. Zhang et al. [16] synthesized polycrystalline $CeO_2$ nanoparticles with size of 4 nm which were coated on CNTs by a simple ultrasonication method under ambient air. Pan et al [17] investigated the CO oxidation properties of $CeO_2$ nanorods, nanowires, nanotubes, and nanocubes. They found that $CeO_2$ nanotubes had the best performance CO oxidation due to the large BET surface area and the novel inner surface. Zhang et al. [18] studied various reaction parameters, such as the content of polyethylene glycol (PEG), molecular weight of PEG, and concentration of KOH, pH value, and sonication time on the as-synthesized polycrystalline $CeO_2$ nanorods by ultrasonication using PEG as a structure-directing agent at room temperature. The content of PEG, molecular weight of PEG, and sonication time was proved to be the crucial factors determining the formation of one-dimensional $CeO_2$ nanorods.

This paper presents the preparation of lanthanide orthophosphate ($LnPO_4$, Ln = La and Ce) nanorods via ultrasonic irradiation without any surfactant or template. Phases, morphologies, and optical properties of these nanomaterials were investigated and discussed.

## 2 Experimental

In the typical preparation of 1D $LnPO_4$ (Ln = La and Ce) nanorods, 0.005 mol $Ln(NO_3)_3{\cdot}6H_2O$ (Ln = La and Ce) and $Na_3PO_4$ were each dissolved in 50 ml distilled water under continuous stirring. Then, the two solutions were mixed, and the pH was adjusted to be 1, 2, and 3 by a concentrated $HNO_3$ solution. Subsequently, the mixtures were processed under ultrasonic irradiation (35 kHz) for 3–6 h. At the conclusion of the process, white green precipitates were synthesized, collected, washed for several times with distilled water and absolute alcohol, and dried at 70 °C for 12 h.

The X-ray powder diffraction (XRD) patterns of all samples were performed on a Philips X'Pert MPD X-ray diffractometer with Cu Kα radiation under a voltage and current of 45 kV and 35 mA, respectively. Fourier transform infrared (FTIR) spectra were recorded on a Perkin Elmer RX spectrophotometer with KBr as a diluting agent and operating in the range of 400–4,000 cm$^{-1}$ with a resolution of 4 cm$^{-1}$. The specific surface area of product was determined by nitrogen adsorption Brunauer–Emett–Teller (BET) method. The BET measurements were performed on a Quantachrome Autosorb-1 MP instrument. Field-emission scanning electron microscopic (FE-SEM) and transmission electron microscopic (TEM) images were taken using a JEOL JSM-6445F and JEM-2010 operated at a beam energy of 15.0 and 200 kV using $LaB_6$ as an electron gun. UV–visible (UV–Vis) spectroscopy was characterized by a Lambda 25 Perkin Elmer spectrometer at room temperature.

## 3 Results and discussion

Figure 1 shows the XRD patterns of the as-prepared $LnPO_4$ (Ln = La and Ce) products at pH 1 under ultrasonic irradiation for 5 h. The diffraction peaks can be readily indexed to be monoclinic phase of $LaPO_4$ and hexagonal $CePO_4$ in consistent with the JCPDS No.32-0493 for $LaPO_4$ and 75-1880 for $CePO_4$ [19]. Peaks of other phases such as $La_2O_3$ and $CeO_2$ are not detected in these XRD patterns, indicating that the products are of high purity and crystallinity. Their lattice parameters can be calculated from plane spacing equations in Eq. (1) for the monoclinic structure and Eq. (2) for hexagonal structure as shown below [20]:

$$\frac{1}{d^2} = \frac{1}{\sin^2\beta}\left[\frac{h^2}{a^2} + \frac{k^2\sin^2\beta}{b^2} + \frac{l^2}{c^2} - \frac{2hl\cos\beta}{ac}\right] \quad (1)$$

$$\frac{1}{d^2} = \frac{4}{3a^2}\left(h^2 + hk + k^2\right) + \frac{1}{c^2}l^2 \quad (2)$$

where $a$, $b$, and $c$ are the lattice unit cells, $h$, $k$, and $l$ are the lattice indexes, $d$ is the plane spacing, and $\beta$ is the angle between the $a$ and $c$ axes (103.6°). Their lattice parameters are $a = 0.67470$ nm, $b = 0.70026$ nm, and $c = 0.64344$ nm for the monoclinic $LaPO_4$ structure and $a = b = 0.69604$ nm and $c = 0.64511$ nm for the hexagonal $CePO_4$ structure, in good agreement with the corresponding standards.

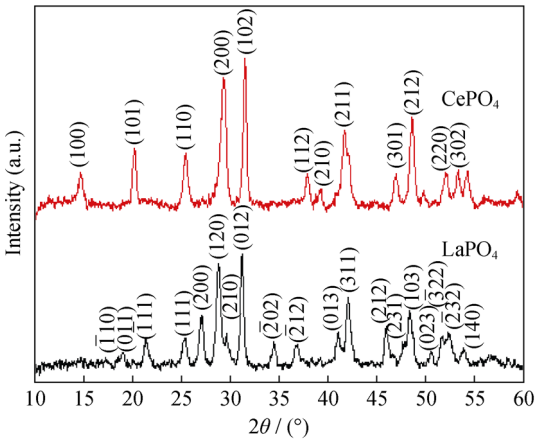


**Fig. 1** XRD patterns of $LnPO_4$ (Ln = La and Ce) samples synthesized in solution at pH 1 by ultrasonic irradiation method for 5 h

The $LaPO_4$ and $CePO_4$ vibrations belonged to tetrahedral $PO_4^{3-}$, by group theory, are $A_1(R) + E(R) + 2F_2(IR + R)$, where $\nu_1(A_1)$ (symmetric stretching vibration frequency) and $\nu_2(E)$ (symmetric bending mode) are Raman active; $\nu_3(F_2)$ (asymmetric stretching frequency) and $\nu_4(F_2)$ (asymmetric bending frequency) have Raman (R) and IR double activity [11]. The symmetry of $PO_4^{3-}$ in the $CePO_4$ crystals decreases from $T_d$ to $C_1$, and the non-IR active modes become IR active. The broad absorption band at 3,460 $cm^{-1}$ in Fig. 2a can be assigned to the vibration of O–H of the water molecules adsorbed on surface of the samples. The other bands are assigned to the vibration of phosphate ($PO_4^{3-}$) groups in wavenumber of 400–1,400 $cm^{-1}$ as shown in Fig. 2b. They can be classified into two groups with bands at 400–700 $cm^{-1}$ and 850–1,100 $cm^{-1}$. The bands at 1,064 $cm^{-1}$ are ascribed to the asymmetric stretching vibration of the $PO_4^{3-}$ groups, and the bands centered at 609 and 536 $cm^{-1}$ belong to the O=P–O and O–P–O bending vibrations of $PO_4^{3-}$ known as the $\nu_4$ mode. The four medium-intensity peaks from 400 to 700 $cm^{-1}$ are due to the bending modes of P–O links in $PO_4^{3-}$ distorted tetrahedrons. Their stretching modes appear as clusters of very strong peaks between 850 and 1,110 $cm^{-1}$ at 955, 993, 1,058, and 1,091 $cm^{-1}$, due to stretching vibrations of $PO_4^{3-}$ in the $\nu_3$ region [9, 11, 21, 22].

Figure 3 shows the difference of length and diameter from the morphological evolution of $LnPO_4$ (Ln = La and Ce) samples prepared at different pH values. Figure 3a–c shows SEM images of the $LaPO_4$ products obtained at pH 3–1. In this research, $LaPO_4$ at pH 3 is a mixture of nanoparticles with sizes below 50 nm and nanorods with 20 nm in diameter and 100–300 nm in length. By SEM observations, the yield of nanoparticles and nanorods is close to 30 % and 70 %. With the pH of the solution decreasing to 2 and 1, the percent of $LaPO_4$ nanoparticles deceases to be less than 10 % at pH 2 and is not detected at pH 1. Only uniform $LaPO_4$ nanorods with 20–25 nm in diameter and 300–600 nm in length are detected at pH 1, and their surfaces are smooth. Figure 3d–f reveals SEM images of $CePO_4$ samples produced by the ultrasonic irradiation method at pH 3–1. The dependence of the morphological evolution for $CePO_4$ samples on pH is the same as for the $LaPO_4$ nanorods. The morphologies of $CePO_4$ at pH 3 are a mixture of 85 % uniform aggregates of parallel aligned nanorods with a diameter of 30–35 nm and length of 500 nm–1 μm and 15 % of agglomerated nanoparticle islands with the size of 200–300 nm. But for $CePO_4$ at pH 2 and 1, agglomerated nanoparticle islands are not detected, showing only $CePO_4$ nanorods. It should be noted that $CePO_4$ at pH 1 is longer than that at pH 2. The length of $CePO_4$ nanorods is 800 nm–1 μm at pH 2 and 1–2 μm at pH 1. In addition, the surface area of $LaPO_4$ and $CePO_4$ nanorods is 63.32 and 35.02 $m^2 \cdot g^{-1}$.

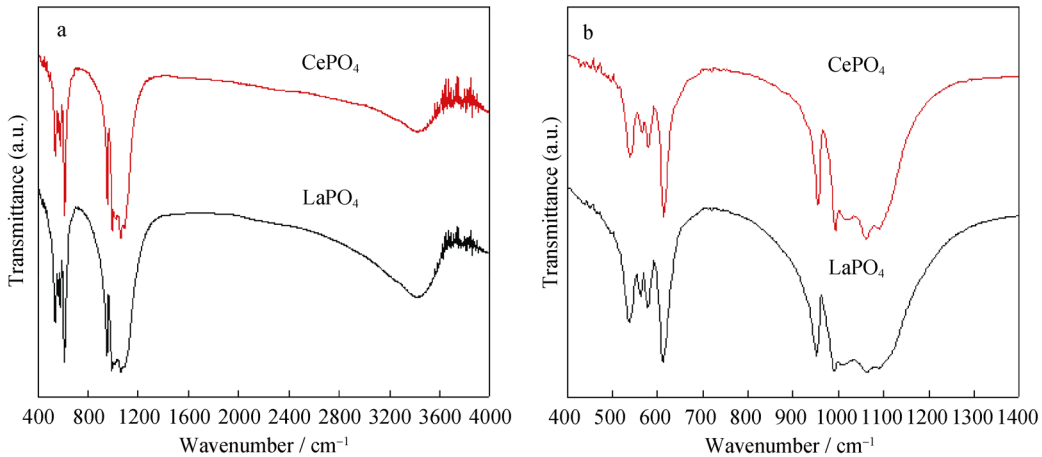


**Fig. 2** FTIR spectra of $LnPO_4$ (Ln = La and Ce) samples synthesized in solution at pH 1 by ultrasonic irradiation method for 5 h: **a** vibration of O-H and **b** vibration of $PO_4^{3-}$

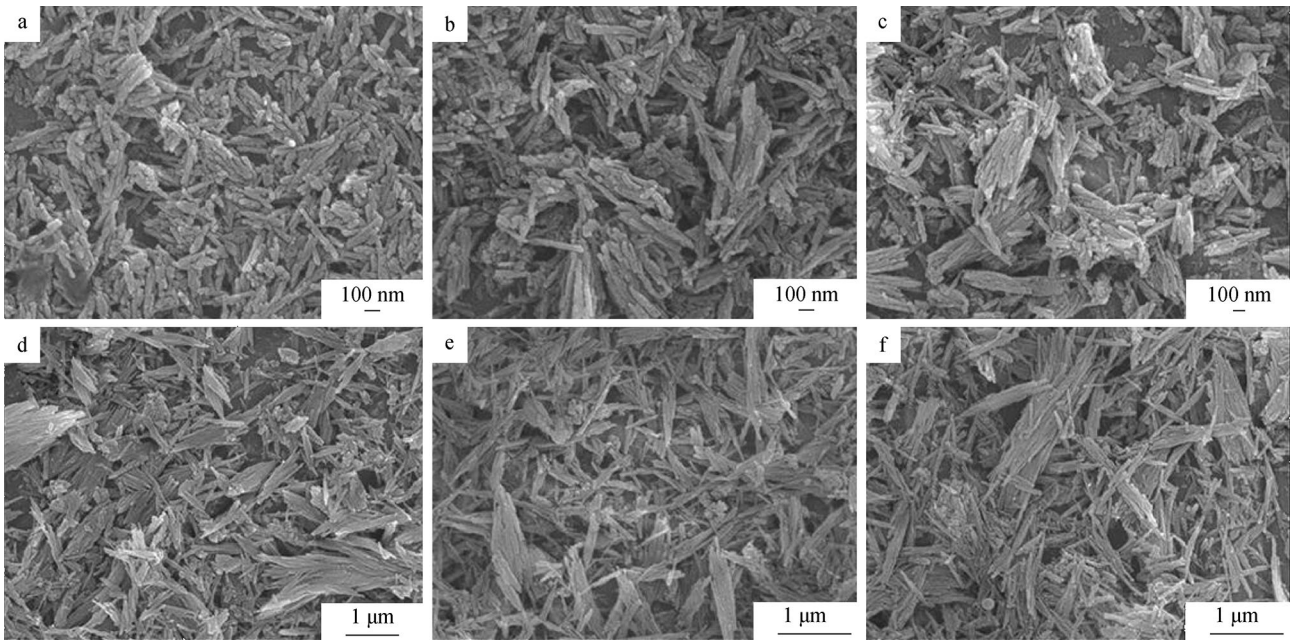


**Fig. 3** SEM images of samples synthesized by ultrasonic irradiation method in solutions with pH of **a** 3, **b** 2, and **c** 1 for $LaPO_4$ nanorods, and **d** 3, **e** and **f** 1 for $CePO_4$ nanorods

From the SEM results, the morphologies of $LnPO_4$ (Ln = La and Ce) nanorods are influenced by the pH of the solution precursor due to the effect of the chemical potential in the same way as previous reports [9, 23, 24]. For example, Zhang and Guan [9] investigated the effects of pH on the morphologies of $LaPO_4$ nanocrystals and found that the 1D $LaPO_4$ nanowires could only be prepared in a pH range of 0.5–1.5. The chemical potential of $LaPO_4$ crystals is higher, which supports the growth of elongated $LaPO_4$ nanocrystals and increases in the rate of hydrolysis and higher acidic conditions. In this research, the chemical potential of the anisotropic 1D $LnPO_4$ (Ln = La and Ce) nanorods is thermodynamically dependent on the acidity of the reaction system. Faster ionic migration usually promotes a reversible pathway between the liquid and solid phases, which promotes ions to occupy at the right positions of the crystal lattices. In conclusion, a high chemical potential of $LnPO_4$ (Ln = La and Ce) crystals in the solutions is another major driving force for the growth of the elongated anisotropic $LnPO_4$ (Ln = La and Ce) nanorods [23].

In addition, the effect of reaction time on the formation of $LnPO_4$ (Ln = La and Ce) nanorods by sonochemical method was investigated by SEM. Figure 4 shows SEM image of $CePO_4$ synthesized by sonochemical method at pH 1 for 3–6 h. The morphologies of $CePO_4$ depend on the reaction time. When reaction time is less than 3 h, the $CePO_4$ nanoparticles with particles size less than 100 nm form. It should be noted that morphologies of $CePO_4$ develop from nanoparticles to nanorods when the reaction time increases to 4 h. $CePO_4$ nanorods have 100–200 nm in length and 50 nm in diameter. The $CePO_4$ nanorods with the length of 1–2 μm were synthesized by sonochemical method at pH 1 for 6 h which is not significantly different for $CePO_4$ nanorods with the reaction time of 5 h. Therefore, the reaction time on the formation of $LnPO_4$ (Ln = La and Ce) nanorods by sonochemical method at pH 1 for 5 h is a suitable condition in synthesis of $LnPO_4$ (Ln = La and Ce) nanorods.

Morphological information of the products was further characterized by transmission electron microscopy (TEM) and high-resolution TEM (HRTEM) as shown in Fig. 5. Figure 5a shows a typical TEM image of the $LaPO_4$ product. It clearly reveals that the product is composed of only nanorods with diameters of 20–60 nm and lengths of 1 μm, respectively. The HRTEM image in Fig. 5b shows that the nanorod is structurally uniform with an interplanar spacing of the (001) planes of $LaPO_4$ and the $LaPO_4$ nanorods grow along the [001] direction [23, 25], with the (−110) plane parallel to the growth direction. Similarly under the same synthetic conditions, $CePO_4$ nanorods with diameters of 20–60 nm and lengths of up to 3 μm can be observed in Fig. 5c. The HRTEM image (Fig. 5d) shows the clearly resolved planes of (−110) which are parallel to the nanorod growth axis [23, 25].

A possible formation mechanism and schematic illustration as shown in Fig. 6 of 1D $LnPO_4$ (Ln = La and Ce) phosphor nanomaterials are explained in Eqs. (3) and (4):

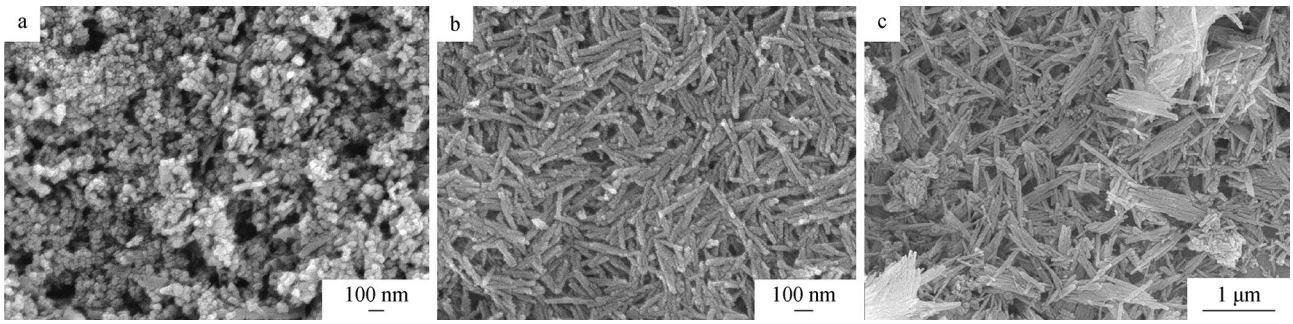


**Fig. 4** SEM images of $CePO_4$ nanorods synthesized at pH of 1 for **a** 3 h, **b** 4 h, and **c** 6 h

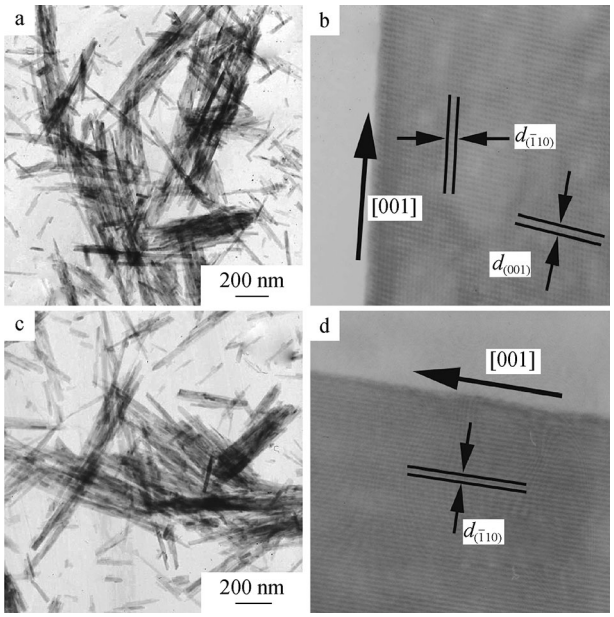


**Fig. 5** TEM and HRTEM images of **a**, **b** $LaPO_4$ nanorods and **c**, **d** $CePO_4$ nanorods

$$PO_4^{3-} + nH^+ \rightarrow H_nPO_4^{(3-n)-} \quad (3)$$

$$Ln^{3+} + H_nPO_4^{(3-n)-} \rightarrow LnPO_4 + nH^+ \quad (4)$$

The $H^+$ reacted with $PO_4^{3-}$ to form $H_nPO_4^{(3-n)-}$. After that the $H_nPO_4^{(3-n)-}$ slowly released $PO_4^{3-}$ which reacted with $Ln^{3+}$ (Ln = La and Ce) to form $LnPO_4$ (Ln = La and Ce) nanorods. The $H^+$ is the key ions in controlling the formation of 1D $LnPO_4$ (Ln = La and Ce) nanorods. By adjusting the pH of the precursors to be 1, the concentration of $H^+$ in the reaction system increases, and the chemical potential also increases. The preferential adsorption of $H^+$ onto certain crystal facets is likely to raise the electrostatic potential on the crystal surfaces of 1D $LnPO_4$ (Ln = La and Ce) nanomaterials. In order to reduce the surface energy, the atoms of the crystal surfaces rearrange themselves [26].

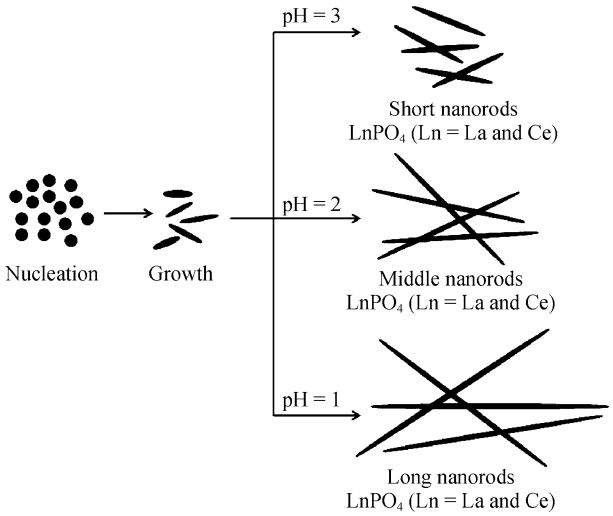


**Fig. 6** Schematic illustration of $LnPO_4$ (Ln = La and Ce) formation

Finally, the 1D $LnPO_4$ (Ln = La and Ce) nanorods are produced.

The UV–Vis spectra of $LnPO_4$ (Ln = La and Ce) nanorods synthesized by the ultrasonic irradiation method are shown in Fig. 7. The absorption spectra of $LaPO_4$ show a strong peak at 227 nm. $La^{3+}$ does not have an electron transfer because it has zero electrons in the 4f shell, and thus there is only one possible optical state of $PO_4^{3-}$ clusters [27]. UV–Vis absorption spectra of $CePO_4$ show two small shoulders at 225 and 278 nm due to the f–d electron transition of $Ce^{3+}$ atoms in the lattice. The energy level for $Ce^{3+}$ shows three electron transitions as $^2F_{5/2} \rightarrow {}^2F_{7/2}$, $^2F_{5/2} \rightarrow {}^2D_{3/2}$, and $^2F_{5/2} \rightarrow {}^2D_{5/2}$. The lowest energy transition ($^2F_{5/2} \rightarrow {}^2F_{7/2}$) is a Laporte forbidden μ to μ transition corresponding to the $f^n$–$f^n$ transition. The other two electron transitions, $^2F_{5/2} \rightarrow {}^2D_{3/2}$ and $^2F_{5/2} \rightarrow {}^2D_{5/2}$, are Laporte allowed *n*f to (*n*–1)f–d transitions. The two major absorption peaks of $CePO_4$ nanorods at 225 and 278 nm are assigned to be $^2F_{5/2} \rightarrow {}^2D_{3/2}$ and $^2F_{5/2} \rightarrow {}^2D_{5/2}$ [28, 29]. Comparing with other reports, UV–Vis absorption spectra of the crystalline $CePO_4$ nanofilaments

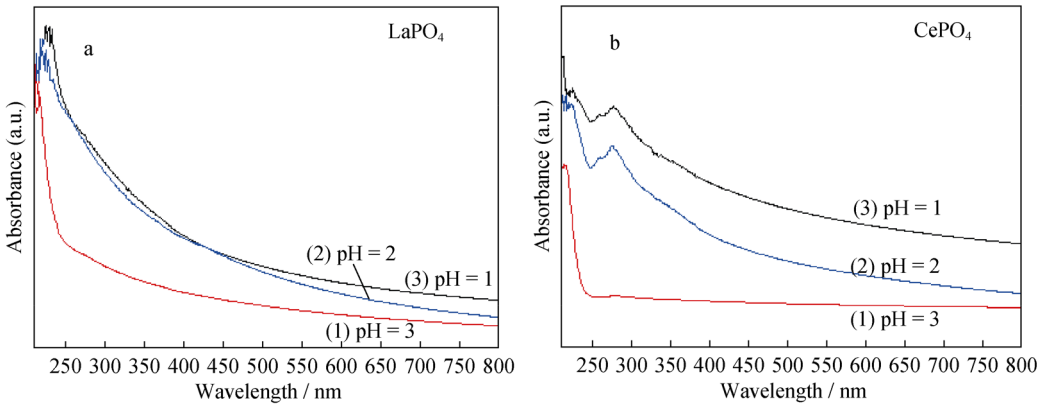


**Fig. 7** UV–Vis spectra of **a** $LaPO_4$ and **b** $CePO_4$ samples synthesized by ultrasonic irradiation method in solutions with pH of 3, 2, and 1

show three peaks with maxima at 213, 256, and 273 nm due to f–d electron transitions in $CePO_4$ [30]. However, the irregular $CePO_4$ nanoparticles show a broad peak at 230–400 nm [31]. Therefore, the optical properties of lanthanide orthophosphate are controlled by morphology of the products.

## 4 Conclusion

In summary, single-crystal $LnPO_4$ (Ln = La and Ce) nanorods were successfully prepared by a simple sonochemical method. It is found that the high aspect ratio of the products is able to be easily controlled by pH values of the solution precursors. This method is a candidate for green chemical synthesis of 1D nanomaterials.

**Acknowledgments** This study was financially supported by the Faculty of Science Research Fund, Faculty of Science, Prince of Songkla University, Thailand.

## References

[1] Qian L, Du W, Gong Q, Qian X. Controlled synthesis of light rare earth phosphate nanowires via a simple solution route. Mater Chem Phys. 2009;114(1):479.
[2] Yin YB, Shao X, Zhao LM, Li WZ. Synthesis and characterization of $CePO_4$ nanowires via microemulsion method at room temperature. Chin Chem Lett. 2009;20(7):857.
[3] Ma L, Chen WX, Zheng YF, Xu ZD. Hydrothermal growth and morphology evolution of $CePO_4$ aggregates by a complexing method. Mater Res Bull. 2008;43(11):2840.
[4] Damien B, Fabienne A, Thibault C, Dimitri S, Didier BA. Solid-state synthesis of monazite-type compounds $LnPO_4$ (Ln = La to Gd). Solid State Sci. 2007;9(5):432.
[5] Ye YX, Wei YH, Sheng WC, Chen M, Hua YQ. Luminescent properties of a new $Nd^{3+}$-doped complex with two different carboxylic acids and pyridine derivative. Rare Met. 2013; 32(5):490.
[6] Ma MG, Zhu JF, Sun RC, Zhu YJ. Hydrothermal synthesis and characterization of $CePO_4$/C core-shell nanorods. Mater Lett. 2009;63(28):2513.
[7] Ma MG, Zhu JF, Cao SW, Chen F, Sun RC. Hydrothermal synthesis of relatively uniform $CePO_4$@$LaPO_4$ one-dimensional nanostructures with highly improved luminescence. J Alloy Compd. 2010;492(1–2):559.
[8] Zhang Y, Guan H. Hydrothermal synthesis and characterization of hexagonal and monoclinic $CePO_4$ single-crystal nanowires. J Cryst Growth. 2003;256(1–2):156.
[9] Zhang Y, Guan H. The growth of lanthanum phosphate (rhabdophane) nanofibers via the hydrothermal method. Mater Res Bull. 2005;40(9):1536.
[10] Nishihama S, Hirai T, Komasawa I. The preparation of rare earth phosphate fine particles in an emulsion liquid membrane system. J Mater Chem. 2002;12(4):1053.
[11] Wang K, Zhang J, Wang J, Fang C, Yu W, Zhao X, Xu H. Growth defects and infrared spectra analysis of $CePO_4$ single crystals. J Appl Crystallogr. 2005;38(4):675.
[12] Zhang D, Du X, Shi L, Gao R. Shape-controlled synthesis and catalytic application of ceria nanomaterials. Dalton Trans. 2012;41(48):14455.
[13] Yu C, Yu M, Li C, Liu X, Yang J, Yang P, Lin J. Facile sonochemical synthesis and photoluminescent properties of lanthanide orthophosphate nanoparticles. J Solid State Chem. 2009; 82(2):339.
[14] Thongtem T, Tipcompor N, Phuruangrat A, Thongtem S. Characterization of $SrCO_3$ and $BaCO_3$ nanoparticles synthesized by sonochemical method. Mater Lett. 2010;64(4):510.
[15] Bhattacharyya S, Gedanken A. A template-free, sonochemical route to porous ZnO nano-disks. Microporous Mesoporous Mater. 2008;110(2–3):553.
[16] Zhang D, Shi L, Fu H, Fang J. Ultrasonic-assisted preparation of carbon nanotube/cerium oxide composites. Carbon. 2006; 44(13):2849.
[17] Pan C, Zhang D, Shi L, Fang J. Template-free synthesis, controlled conversion, and CO oxidation properties of $CeO_2$ nanorods, nanotubes, nanowires, and nanocubes. Eur J Inorg Chem. 2008;2008(15):2429.
[18] Zhang D, Fu H, Shi L, Pan C, Li Q, Chu Y, Yu W. Synthesis of $CeO_2$ nanorods via ultrasonication assisted by polyethylene glycol. Inorg Chem. 2007;46(7):2446.
[19] Powder Diffraction File, JCPDS-ICDD, 12 Campus Boulevard, Newtown Square, USA, 2001.
[20] Suryanarayana C, Norton MG. X-Ray Diffraction: a Practical Approach. New York: Plenum Press; 1998. 251.
[21] Sumaletha N, Rajesh K, Mukundan P, Warrier KGK. Environmentally benign sol–gel derived nanocrystalline rod shaped calcium doped cerium phosphate yellow–green pigment. J Sol–Gel Sci Technol. 2009;52(2):242.

[22] Yang M, You H, Zheng Y, Liu K, Jia G, Song Y, Huang Y, Zhang L, Zhang H. Hydrothermal synthesis and luminescent properties of novel ordered sphere $CePO_4$ hierarchical architectures. Inorg Chem. 2009;48(24):11559.
[23] Zhang YW, Yan ZG, You LP, Si R, Yan CH. General synthesis and characterization of monocrystalline lanthanide orthophosphate nanowires. Eur J Inorg Chem. 2003;2003(24):4099.
[24] Wang X, Gao M. A facile route for preparing rhabdophane rare earth phosphate nanorods. J Mater Chem. 2006;16(14):1360.
[25] Cao M, Hu C, Wu Q, Guo C, Qi Y, Wang E. Controlled synthesis of $LaPO_4$ and $CePO_4$ nanorods/nanowires. Nanotechnology. 2005;16(2):282.
[26] Phuruangrat A, Ekthammathat N, Thongtem S, Thongtem T. Preparation of $LaPO_4$ nanowires with high aspect ratio by a facile hydrothermal method and their photoluminescence. Res Chem Intermed. 2013;39(3):1363.
[27] Mishra KC, Osterloh I, Anton H, Hannebauer B, Schmidt PC, Johnson KH. First principles investigation of host excitation of $LaPO_4$, $La_2O_3$ and $AlPO_4$. J Lumin. 1997;72–74:144.
[28] Zhang F, Wong SS. Ambient large-scale template-mediated synthesis of high-aspect ratio single-crystalline, chemically doped rare-earth phosphate nanowires for bioimaging. ACS Nano. 2010;4(1):99.
[29] Fang YP, Xu AW, Song RQ, Zhang HX, You LP, Yu JC, Liu HQ. Systematic synthesis and characterization of single-crystal lanthanide orthophosphate nanowires. J Am Chem Soc. 2003;125(51):16025.
[30] Xing Y, Li M, Davis SA, Patil AJ, Mann S. Synthesis of cerium/cobalt phosphate nanostructures in catanionic reverse micelles. Soft Matter. 2006;2(7):603.
[31] Zhang Y, Wang J, Zhang T. Novel Ca-doped $CePO_4$ supported ruthenium catalyst with superior catalytic performance for aerobic oxidation of alcohols. Chem Commun. 2011;47(18):5307.